Journal of Theoretical and Applied Mechanics, Sofia, 2008, vol. 38, Nos 1–2, pp. 7–24

# FINITE ELEMENT MODELLING OF THERMO-ELASTO-PLASTIC WATER SATURATED POROUS MATERIALS*

Lorenzo Sanavia
*Dipartimento di Costruzioni e Trasporti, Università degli Studi di Padova, Via Marzolo 9, 35-131 Padova, Italy,*
e-mail: lorenzo.sanavia@unipd.it

Bertrand François
*Soil Mechanics Laboratory, Ecole Polytechnique Fédérale Lausanne, EPFL, 1015 Lausanne, Switzerland,*
e-mail: bertrand.francois@epfl.ch

Roberto Bortolotto, Loris Luison
*Dipartimento di Costruzioni e Trasporti, Università degli Studi di Padova, Via Marzolo 9, 35-131 Padova, Italy,*
e-mails: roberto.bortolotto@unipd.it, loris.luison@unipd.it

Lyesse Laloui
*Soil Mechanics Laboratory, Ecole Polytechnique Fédérale Lausanne, EPFL, 1015 Lausanne, Switzerland,*
e-mail: lyesse.laloui@epfl.ch

*Dedicated to Professor Bernhard A. Schrefler on the occasion of his 65th birthday*

[Received 10 July 2007. Accepted 25 February 2008]

Abstract.The purpose of this paper is to present a new finite element formulation for the hydro-thermo-mechanical analysis of elasto-plastic multiphase materials based on Porous Media Mechanics.

To this end, the ACMEG-T thermo-plastic constitutive model for saturated soils has been implemented in the finite element code COMES-GEO.

Validation of the implemented model is made by selected comparison

*The authors would like to thank the University of Padua (UNIPD 60A09-5407/06), the Foundation "Cassa di Risparmio di Padova e Rovigo" and the Swiss State Secretariat for Education and Research SER (*Grant* OFES C04.0021) for their financial support.

between model simulation and experimental results for different combinations of thermo-hydro-mechanical loading paths. A case of non-isothermal elasto-plastic consolidation is also shown.
KEY WORDS: thermo-elastoplasticity, water saturated porous materials, finite element method, isotropic compression test, triaxial test, consolidation.

## 1. Introduction

In recent years, increasing interest in thermo-hydro-mechanical analysis of geomaterials is observed, because of a wide spectrum of their engineering applications. Typical examples belong to Environmental Geomechanics, where some challenging problems are of interest, as for example the case of the nuclear waste isolation and of geothermal structures.

A step in the development of a suitable physical, mathematical and numerical model for the simulation of geo-environmental engineering problems is presented here. To this end, the general ACMEG-T thermo-elastoplastic constitutive model for saturated soils [1], [2] has been implemented in the finite element code COMES-GEO for the analysis of non-isothermal elasto-plastic porous materials [3].

In this paper we summarize the mathematical formulation for non-isothermal elasto-plastic water saturated porous materials in Section 2. The material is considered as made of a solid phase and open pores, which are filled with one fluid, and is modelled as a deforming porous continuum where heat conduction and convection and water advection are taken into account [4], [5]. The elasto-plastic behaviour of the solid skeleton is assumed homogeneous and isotropic; the effective stress state is limited by two temperature dependent yield surfaces, with non associated plastic flow, as presented in Section 3. The macroscopic balance equations are discretized in space and time within the finite element method for coupled problems, e.g. [4]. In particular, a Galerkin procedure is used for the discretisation in space, and the Generalised Trapezoidal Method for the time integration (see Section 5). Small strains and quasi-static loading conditions are assumed.

Validation of the implemented model by selected comparison between model simulation and experimental results for different combinations of thermo-hydro-mechanical loading paths is presented in Section 6. A case of non-isothermal elastic and elasto-plastic consolidation is described.

A review of non-isothermal thermo-hydro-mechanical models and of thermo-elasto-plastic constitutive formulations for soils is beyond the scope of this paper; the interested reader can find it in [3], [4] and [1], [2], respectively.

## 2. Macroscopic balance equations

A full mathematical model necessary to simulate Thermo-Hydro-Mechanical (THM) transient behaviour of fully and partially saturated porous media was developed in [4], [5] and [6] using averaging theories following [7] (see also [8]). The model for water saturated porous materials is briefly summarized in the present section for sake of completeness.

The porous medium is treated as two-phase system composed of the solid skeleton ($s$) with open voids filled with water ($w$).

At the macroscopic level the porous material is modelled by a substitute continuum of volume $B$ with boundary $\partial B$ that simultaneously fills the entire domain, instead of the real fluid and the solid which fill only a part of it. In this substitute continuum each constituent $\pi$ has a reduced density which is obtained through the volume fraction $\eta^{\pi}(\boldsymbol{x},t) = dv^{\pi}(\boldsymbol{x},t)/dv(\boldsymbol{x},t)$, where $\boldsymbol{x}$ is the vector of the spatial coordinates and $t$ is the current time ($\pi = s, w$). Heat conduction, heat convection and water flow due to pressure gradient inside the pores are taken into account. The solid is deformable and non-polar, and the fluid, solid and thermal fields are coupled. Local thermal equilibrium between solid matrix and liquid phase is assumed. The state of the medium is described by pore water pressure $p^w$, absolute temperature $T$ and displacements of the solid matrix $\mathbf{u}$. Pore pressure is defined as compression positive for water, while stress is defined as tension positive for the solid phase.

Before presenting the balance equations used in the present case, it is useful to mention that the full mathematical model and its implementation in the COMES-GEO finite element code consider the soil as a non-isothermal three-phase media in which not only water but also a gas phase may fill the void space. In this complete formulation, which is not addressed here, the gas phase is modelled as an ideal gas mixture composed of dry air and water vapour. Phase changes of water (evaporation-condensation, adsorption-desorption) and latent heat transfer are considered [4], [5], [6], [8]. A recent development which considers the air dissolved in the liquid phase and its desorption at lower water pressure is presented in [9].

The balance equations of the implemented model are now summarized. These equations are obtained assuming the porous medium to be constituted of incompressible solid and water constituent; the process is considered as quasi-static and developed in the geometrically linear framework.

The linear momentum balance equation of the mixture in terms of effective Cauchy's stress $\boldsymbol{\sigma}'(\boldsymbol{x},t)$ assumes the form,

$$\operatorname{div}\left(\boldsymbol{\sigma}' - p^w\,\mathbf{1}\right) + \rho\,\mathbf{g} = \mathbf{0}, \tag{1}$$

where $\rho = [1-n]\,\rho^s + n\rho^w$ is the density of the mixture, $n(\boldsymbol{x}$,t) the porosity, $\mathbf{g}$ is the gravity acceleration vector and $\mathbf{1}$ the second order identity tensor.

The mass conservation equation for the water is,

$$\rho^w \operatorname{div} \boldsymbol{v}^s - \operatorname{div}\left(\rho^w \frac{\mathbf{k}}{\mu^w}\left[\operatorname{grad}\left(p^w\right) - \rho^w \mathbf{g}\right]\right) - \rho^w \beta_{sw} \frac{\partial T}{\partial t} = 0, \tag{2}$$

where $\boldsymbol{v}^s$ is the solid velocity, $\mathbf{k}(\boldsymbol{x}, t)$ is the intrinsic permeability tensor and $\mu^w(\boldsymbol{x}, t)$ the water viscosity. $\beta_{sw}(\boldsymbol{x}, t) = [1-n]\beta_s + n\beta_w$ is the cubic thermal expansion coefficient of the medium, $\beta_s$ and $\beta_w$ being the solid and water cubic thermal expansion coefficient, respectively. In equation (2), the water flux has been described using the Darcy law.

The energy balance equation of the mixture has the following form,

$$\left(\rho C_p\right)_{\mathit{eff}} \frac{\partial T}{\partial t} - \left(\rho^w C_p^w \frac{\mathbf{k}}{\mu^w}\left[\operatorname{grad}\left(p^w\right) - \rho^w g\right]\right) \cdot \operatorname{grad} T - \operatorname{div}\left(\chi_{\mathrm{eff}} \operatorname{grad} T\right) = 0, \tag{3}$$

where $\left(\rho C_p\right)_{\mathit{eff}} = (1-n)\,\rho^s C_p^s + n\rho^w C_p^w$ is the effective thermal capacity of porous medium, $C_p^s$ and $C_p^w$ the specific heat of solid and water, respectively, and $\chi_{\mathit{eff}}$ the effective thermal conductivity of the porous medium. This balance equation takes into account the heat transfer through conduction and convection (see [4], [5]) and neglects the terms related to the mechanical work induced by density variations due to temperature changes of the phases and induced by volume fraction changes.

## 3. Constitutive equations

The thermo-elastoplastic behaviour of the solid skeleton is described by the general ACMEG-T thermo-plastic constitutive model for water saturated soils developed in [1], [2], [10] within the rate-independent elasto-plasticity theory for geometrically linear problems.

The most relevant experimental results for the constitutive description of the soil behaviour will be summarized in the following, before the description of the constitutive model (see e.g. [2] for a comprehensive description).

When studying thermo-mechanical behaviour of soil, some specific experimental observations must be considered in the constitutive development. In particular, irreversible processes induced by temperature changes may induce thermo-plastic processes in soils. These irreversible effects strongly depend on the stress level measured in terms of OverConsolidation Ratio (OCR). Under Normally Consolidated conditions (NC), soils contracts when it is heated and

a significant part of this deformation is irreversible upon cooling. The behaviour over the whole cycle indicates the irreversibility of strain due to thermal loading, which is representative of thermal hardening. On the contrary, the highly overconsolidated states produce mainly reversible dilation when heated. Between these states, an intermediate one (low OCR) first produces dilation, then a tendency toward contraction on heating paths.

In addition, several results from the literature show a decrease in the preconsolidation pressure with increasing temperature. Finally, under undrained conditions, when soil is heated, the higher thermal expansion of water than that of the solid skeleton induces pore water pressure increase. Indeed, a temperature increase tends to enhance the pore space of the material proportionally to the thermal expansion coefficient of the solid skeleton. Nevertheless, this effect is more than counterbalanced by the thermal dilation of water. Moreover, when the soil tends to collapse during heating (due to thermo-plastic behaviour of NC soils), the undrained conditions make the decrease of pore space impossible, which provokes an additional increase in pore water pressure.

The ACMEG-T model considers a non-linear thermo-elasticity coupled with a multi-dissipative thermo-plasticity in order to reproduce all the thermo-mechanical features of behaviour exposed above.

The elastic part of the deformation is expressed as following:

$$d\boldsymbol{\varepsilon}^e = \mathbf{D}^{-1} d\boldsymbol{\sigma}' + \boldsymbol{\beta}_{\mathrm{T}} dT, \tag{4}$$

$\mathbf{D}$ is the mechanical elastic tensor defined by the non-linear bulk and shear modulus, $K$ and $G$, respectively,

$$K = K_{ref} \left( \frac{p'}{p'_{ref}} \right)^{n^e}, \qquad G = G_{ref} \left( \frac{p'}{p'_{ref}} \right)^{n^e}, \tag{5}$$

$p'$ is the effective mean stress, $n^e$ the non-linear elasticity exponent, $p'_{ref}$ the reference pressure, $K_{ref}$ and $G_{ref}$ the bulk and shear modulus at the reference pressure, respectively. $\boldsymbol{\beta}_{\mathrm{T}}$ is the thermal expansion tensor. Considering an isotropic thermal dilatation, one can express the thermal expansion tensor as $\boldsymbol{\beta}_{\mathrm{T}} = \frac{1}{3}\beta_s \mathbf{1}$ with $\beta_s$ being the volumetric thermal expansion coefficient of the solid skeleton.

The material plasticity is induced by two coupled mechanisms: an isotropic and a deviatoric mechanism. The yield functions of the two mechanical thermo-plastic mechanisms, $f_{iso}$ and $f_{dev}$, representing the isotropic

and deviatoric yield limits, respectively, restricting the effective stress state $\boldsymbol{\sigma}'(\boldsymbol{x}, t)$, take the following expressions (Fig. 1):

$$f_{iso} = p' - p'_c r_{iso}, \qquad f_{dev} = q - Mp' \left(1 - b \ln \frac{dp'}{p'_c}\right) r_{dev} = 0, \tag{6}$$

where $q$ is the deviatoric stress. Each of the yield limits evolves through the generation of plastic strains. During loading, the volumetric plastic strain governs the evolution of $p'_c$ and $r_{iso}$, while deviatoric plastic strains control the evolution of $r_{dev}$.

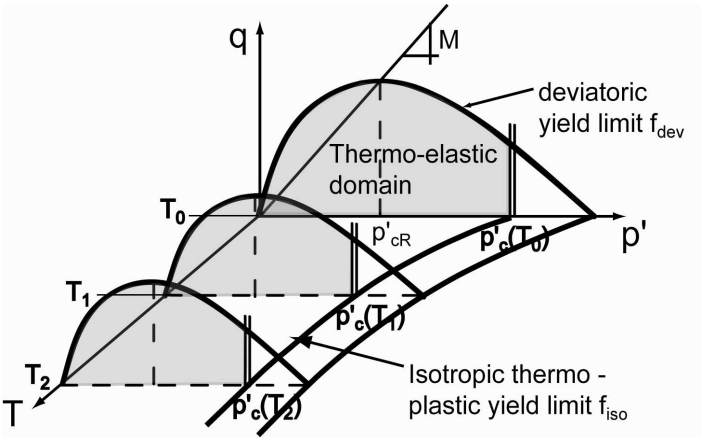


Fig. 1. Yield limits for the ACMEG-T thermo-mechanical elasto-plastic framework. $q$: shear stress, $p'$: mean effective stress, $T$: temperature, $p'_c$: critical pressure

The preconsolidation pressure, $p'_c$, depends on the volumetric plastic strain $\varepsilon_v^p$ and temperature [1]:

$$p'_c = p'_{c_0 T_0} \exp\left\{\beta \varepsilon_v^P\right\} \left\{1 - \gamma_T \log\left[T/T_0\right]\right\}, \tag{7}$$

where $p'_{c_0 T_0}$ is the initial value of the preconsolidation pressure at the reference temperature, $T_0$, while $\beta$ and $\gamma_T$ are material parameters.

$r_{iso}$ and $r_{dev}$ correspond to the degree of plastification (mobilised hardening) of the isotropic and deviatoric yield limits, respectively. This enables a progressive evolution of the isotropic yield limit during loading and a partial comeback of this limit during unloading. The evolution of $r_{iso}$ during loading is linked to the volumetric plastic strain induced by the isotropic mechanism $\varepsilon_v^{p,iso}$:

$$r_{iso} = r_{iso}^e + \frac{\varepsilon_v^{p,iso}}{c + \varepsilon_v^{p,iso}}, \tag{8}$$

where $c$ and $r^e_{iso}$ are material parameters. In the same way, the evolution of $r_{dev}$ during loading is linked to the deviatoric plastic strain $\varepsilon^p_d$:

$$r_{dev} = r^e_{dev} + \frac{\varepsilon^p_d}{a + \varepsilon^p_d}, \tag{9}$$

where $a$ and $r^e_{dev}$ are material parameters. For more completeness about the equations of this progressive mobilised hardening, the readers may refer to [11], or more recently, to [10].

The deviatoric yield limit described by equation (6) counts three additional material parameters. $b$ and $d$ govern the shape of the yield limit and $M$ is the slope of critical state line, which may depend on temperature,

$$M = M_0 - g\,(T - T_0)\,, \qquad M_0 = \frac{6\sin\phi'_0}{3 - \sin\phi'_0}, \tag{10}$$

where $\phi'_0$ is the friction angle at critical state at the reference temperature $T_0$ and $g$ defines the linear evolution of $M$ with temperature $T$.

The flow rule of the isotropic mechanism is associated, while the deviatoric one is not and assumes the following forms:

$$\mathrm{d}\boldsymbol{\varepsilon}^{p,iso} = \lambda^p_{iso}\frac{\partial g_{iso}}{\partial \boldsymbol{\sigma}'} = \frac{\lambda^p_{iso}}{3}\mathbf{1}, \tag{11}$$

$$\mathrm{d}\boldsymbol{\varepsilon}^{p,dev} = \lambda^p_{dev}\frac{\partial g_{dev}}{\partial \boldsymbol{\sigma}'} = \lambda^p_{dev}\frac{1}{Mp'}\left[\frac{\partial q}{\partial \boldsymbol{\sigma}'} + \alpha\left(M - \frac{q}{p'}\right)\frac{1}{3}\mathbf{1}\right]. \tag{12}$$

The plastic multipliers, $\lambda^p_{iso}$ and $\lambda^p_{dev}$, are determined using Prager's consistency equation for multi-dissipative plasticity [12], [13], [14]. $\alpha$ is a material parameter.

## 4. Initial and boundary conditions

For the model closure the initial and boundary conditions are needed. The initial conditions specify the full fields of state variables at time $t = t_0$ in the whole domain and on its boundary as: $p^w = p^w_0$, $T = T_0$, $\mathbf{u} = \mathbf{u}_0$ on $B \cup \partial B$.

The Boundary Conditions (BCs) can be of Dirichlet's type on $\partial B_\pi$ for $t \geq t_0$:

$$p^w = \hat{p}^w \ \text{ on } \ \partial B_w, \qquad T = \hat{T} \ \text{ on } \ \partial B_T, \qquad \mathbf{u} = \hat{\mathbf{u}} \ \text{ on } \ \partial B_u \tag{13}$$

or of Neumann' BCs type on $\partial B_\pi^q$ for $t \geq t_0$:

$$
\begin{aligned}
&\rho^w \frac{\mathbf{k}}{\mu^w} \left[ -\operatorname{grad}(p^w) + \rho^w \mathbf{g} \right] \cdot \mathbf{n} = q^w \quad \text{on } \partial B_w^q, \\
&\chi_{\mathit{eff}} \operatorname{grad}(T) \cdot \mathbf{n} = \alpha_c (T - T_\infty) + q^T \quad \text{on } \partial B_T^q, \\
&\boldsymbol{\sigma} \cdot \mathbf{n} = \mathbf{t} \quad \text{on } \partial B_t^q,
\end{aligned}
\tag{14}
$$

where $\mathbf{n}(\boldsymbol{x}, t)$ is the unit normal vector, $q^w(\boldsymbol{x}, t)$ and $q^T(\boldsymbol{x}, t)$ are the imposed water and heat fluxes, respectively, and $\mathbf{t}(\boldsymbol{x}, t)$ is the imposed traction vector related to the total Cauchy stress tensor $\boldsymbol{\sigma}(\boldsymbol{x}, t)$. $\alpha_c(\boldsymbol{x}, t)$ is the convective heat transfer coefficient and $T_\infty(\boldsymbol{x}, t)$ is the temperature in the far field.

## 5. Finite element formulation

The finite element model is derived by applying the Galerkin procedure for the spatial integration and the Generalised Trapezoidal Method for the time integration of the weak form of the balance equations of Section 2 (e.g. [4]). In particular, after spatial discretisation within the isoparametric formulation, the following non-symmetric, non-linear and coupled system of equation is obtained,

$$
\begin{bmatrix} \mathbf{C}_{ww} & \mathbf{C}_{wt} & \mathbf{C}_{wu} \\ \mathbf{C}_{tw} & \mathbf{C}_{tt} & \mathbf{C}_{tu} \\ \mathbf{0} & \mathbf{0} & \mathbf{0} \end{bmatrix} \frac{\partial}{\partial t} \begin{bmatrix} \bar{\mathbf{p}}^w \\ \bar{\mathbf{T}} \\ \bar{\mathbf{u}} \end{bmatrix} + \begin{bmatrix} \mathbf{K}_{ww} & \mathbf{K}_{wt} & \mathbf{0} \\ \mathbf{K}_{tw} & \mathbf{K}_{tt} & \mathbf{0} \\ \mathbf{K}_{uw} & \mathbf{K}_{ut} & \mathbf{K}_{uu} \end{bmatrix} \begin{bmatrix} \bar{\mathbf{p}}^w \\ \bar{\mathbf{T}} \\ \bar{\mathbf{u}} \end{bmatrix} = \begin{bmatrix} \mathbf{f}_w \\ \mathbf{f}_t \\ \mathbf{f}_u \end{bmatrix},
\tag{15}
$$

where the solid displacements $\mathbf{u}(\boldsymbol{x}, t)$, the pore water pressure $p^w(\boldsymbol{x}, t)$ and the temperature $T(\boldsymbol{x}, t)$ are expressed in the whole domain by global shape function matrices $\mathbf{N}_u(\boldsymbol{x})$, $\mathbf{N}_w(\boldsymbol{x})$, $\mathbf{N}_T(\boldsymbol{x})$ and the nodal value vectors $\bar{\mathbf{u}}(t)$, $\bar{\mathbf{p}}^w(t)$, $\bar{\mathbf{T}}(t)$.

In a more concise form the previous system is written as $\mathbf{G}(\mathbf{X}) = \mathbf{C}\dfrac{\partial \mathbf{X}}{\partial t} + \mathbf{K}\mathbf{X} - \mathbf{F} = \mathbf{0}$, where $\mathbf{X} = \left[\bar{\mathbf{p}}^w, \bar{\mathbf{T}}, \bar{\mathbf{u}}\right]^T$ is the solution vector.

Finite differences in time are used for the solution of the initial value problem over a finite time step $\Delta t = t_{n+1} - t_n$. Following the Generalised Trapezoidal Method, equations (15) are rewritten at time $t_{n+1}$ using the relationships

$$
\left.\frac{\partial \mathbf{X}}{\partial t}\right|_{n+\theta} = \frac{\mathbf{X}_{n+1} - \mathbf{X}_n}{\Delta t}, \quad \mathbf{X}_{n+\theta} = [1-\theta]\mathbf{X}_n + \theta \mathbf{X}_{n+1}, \quad \text{with } \theta \in [0, 1].
\tag{16}
$$

Linearized analysis of accuracy and stability suggest the use of $\theta \geq 0.5$. In the example section, implicit one-step time integration has been performed ($\theta = 1$).

After time integration the non-linear system of equations is linearized, thus obtaining the equations system that can be solved numerically (in compact form)

$$\left.\frac{\partial \mathbf{G}}{\partial \mathbf{X}}\right|_{\mathbf{X}^i_{n+1}} \Delta \mathbf{X}^{i+1}_{n+1} \cong -\mathbf{G}(\mathbf{X}^i_{n+1}) \tag{17}$$

with the symbol $(\bullet)^{i+1}_{n+1}$ to indicate the current iteration $(i+1)$ in the current time step $(n+1)$ and where $\partial\mathbf{G}/\partial\mathbf{X}$ is the Jacobian matrix. Details concerning the matrices and the residuum vector of the linearized equations system can be found in [3].

Owing to the strong coupling between the mechanical, thermal and the pore fluid fields, a monolithic solution of (17) is preferred using a Newton scheme. Finally, the solution vector $\mathbf{X}$ is then updated by the incremental relationship $\mathbf{X}^{i+1}_{n+1} = \mathbf{X}^i_{n+1} + \Delta\mathbf{X}^{i+1}_{n+1}$.

## 6. Numerical results

In this section, the validation of the implementation of ACMEG-T thermo-plastic constitutive model for saturated soils is presented and discussed by comparison between experimental and finite element results at element level and by solving a reference case of non-isothermal consolidation taken from the literature [15].

### 6.1. Validation at the element level

The first set of examples deals with the simulation of isothermal isotropic and triaxial compression tests. The case of isotropic compression is represented by a mechanical compression test on silty sand under saturated conditions [16]. This test is simulated with an axisymmetric finite element analysis under isotropic load: $\sigma'_r = \sigma'_z = \sigma'_\theta = p'$, $\tau_{rz} = \tau_{z\theta} = \tau_{\theta r} = 0$. The initial effective stress is characterized by a mean compressive pressure $p' = -10$ kPa and a deviatoric stress $q = 0$ kPa. This compression test consists of a [$-100$; $-10$; $-200$; $-10$; $-550$ kPa] loading-unloading cycle. The material parameters used in the computation are listed in Table 1.

The analysis was performed discretizing the geometry successively with one and one hundred linear element(s) and with one 8-node element. The comparison between the experimental and the finite element results shows a good agreement, independently of the spatial discretisation (Fig. 2). This first very simple example of numerical simulation under isotropic compression path shows the capability of the ACMEG-T model to reproduce the progressive

plasticity of materials. The transition between purely elastic behaviour and the total mobilisation of plasticity is smooth as experimentally observed.

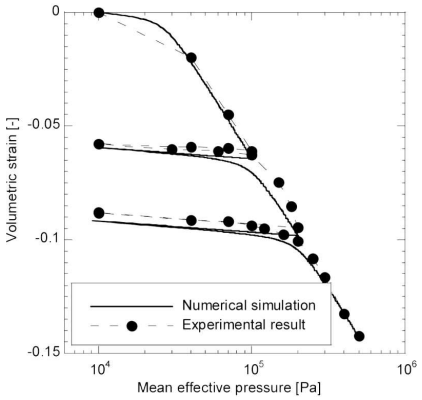


Fig. 2. Isothermal isotropic compression test: Comparison between the experimental and the finite element results

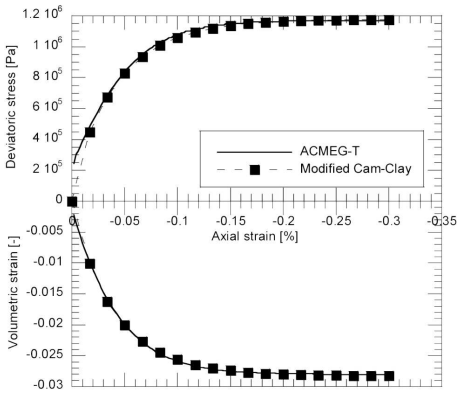


Fig. 3. Isothermal triaxial compression test: Comparison between Modified Cam-Clay simulation and the finite element results

The second example simulates triaxial compression test on normally consolidated sample submitted to an initial mean pressure $p'$ of $-800$ kPa, without deviatoric component and by imposing a vertical displacement of the upper surface. This example uses a fictive material for which the material parameters have been arbitrary chosen to correspond to well-known Modified Cam-Clay model. Indeed, ACMEG-T model can be seen has an extension of the Modified Cam-Clay model. The material parameters used in the computation are listed in Table 1. Figure 3 shows that, by selecting adequate parameters, the ACMEG-T response gives identical results than the Modified Cam-Clay simulated with a commercial code.

These two first examples tend, first, to validate the implementation of the isothermal part of ACMEG-T model in the COMES-GEO code and, secondly, to prove the capability of the constitutive model to reproduce the response of soils submitted to classical mechanical paths.

As a second part of the validation process, the next simulations show the efficiency of the model implemented in COMES-GEO to reproduce soil behaviours under non-isothermal conditions. To this end, two sets of experiments are simulated numerically. The first one consists of heating-cooling cycles on soils having different degree of consolidation (OCR = 1; 2; 6), as performed by [17]. The material parameters are listed in Table 1. The initial mean pressure

Table 1. Material parameters used in the computation of the (1) Isothermal isotropic compression, (2) Isothermal triaxial compression, (3) Heating-cooling cycle, (4) Triaxial compression at two different temperatures

| | Elastic parameters | | | | | Isotropic plastic parameters | | | | | Deviatoric plastic parameters | | | | | | | |
|---|---|---|---|---|---|---|---|---|---|---|---|---|---|---|---|---|---|---|
| | $K_{ref}$ | $G_{ref}$ | $p'_{ref}$ | $n^e$ | $\beta_s$ | $p'_{c_0T_0}$ | $\beta$ | $c$ | $r^e_{iso}$ | $\gamma_T$ | $b$ | $d$ | $\phi'_0$ | $\alpha$ | $a$ | $r^e_{dev}$ | $g$ |
| | [MPa] | [MPa] | [MPa] | [–] | [$K^{-1}$] | [MPa] | [–] | [–] | [–] | [–] | [–] | [–] | [°] | [–] | [–] | [–] | [–] |
| (1) | 460 | 690 | −1 | 1 | / | −0.028 | −22 | 0.001 | 0.001 | / | / | / | / | / | / | / | / |
| (2) | 131 | 78 | −1 | 1 | / | −0.8 | −44 | 0.001 | 1 | / | 1 | 2 | −25 | 1 | 0.001 | 1 | / |
| (3) | 150 | 130 | −1 | 1 | 3E–5 | −6 | −47 | 4E–4 | 0.01 | 0.18 | / | / | / | / | / | / | / |
| (4) | 70 | 30 | −1 | 0.68 | / | −0.6 | −21 | 0.055 | 0.01 | 0.075 | 0.5 | 2.75 | −22 | 2 | 0.0035 | 0.1 | 2.9E–5 |

Table 2. Material parameters used in the computation of the non-isothermal consolidation example – (1) Thermo-elastic case, (2) Thermo-elastoplastic case

| | Elastic parameters | | | | | Isotropic plastic parameters | | | | | Diffusive law | | | | | | |
|---|---|---|---|---|---|---|---|---|---|---|---|---|---|---|---|---|---|
| | $K_{ref}$ | $G_{ref}$ | $p'_{ref}$ | $n^e$ | $\beta_s$ | $p'_{c_0T_0}$ | $\beta$ | $c$ | $r^e_{iso}$ | $\gamma_T$ | $\rho^s$ | $\rho^w$ | $n$ | $k$ | $\lambda_s$ | $c_s$ | $\lambda_w$ | $c_w$ |
| | [MPa] | [MPa] | [MPa] | [–] | [$K^{-1}$] | [Pa] | [–] | [–] | [–] | [–] | [kg/ [$m^3$]] | [kg/ $m^3$] | [–] | [$m^2$] | [W/ (m K)] | [J/ (kg K)] | [W/ (m K)] | [J/ (kg K)] |
| (1) | 10 | 2.14 | −1 | 0 | 9E–7 | –1E10 | / | / | 1 | 0 | 2000 | 1000 | 0.2 | 4.6E–17 | 0.84 | 16760 | 0.6 | 4181 |
| (2) | 10 | 2.14 | −1 | 0 | 9E–7 | −800 | −20 | 0.001 | 0.001 | 0.2 | 2000 | 1000 | 0.2 | 4.6E–17 | 0.84 | 16760 | 0.6 | 4181 |

is of -6.0 MPa, -3.0 MPa and −1.0 MPa for OCR = 1; 2; 6, respectively.

The comparison between the experimental and the finite element results shows a very good agreement, as it can be seen in Fig. 4. This specific response of soil depending on the stress state is very representative of thermo-plastic effects, as already mentioned in Section 3.

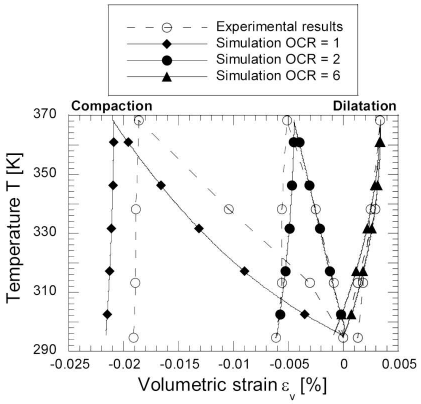


Fig. 4. Heating-cooling at different OCR: Comparison between the experimental [17] and the finite element results

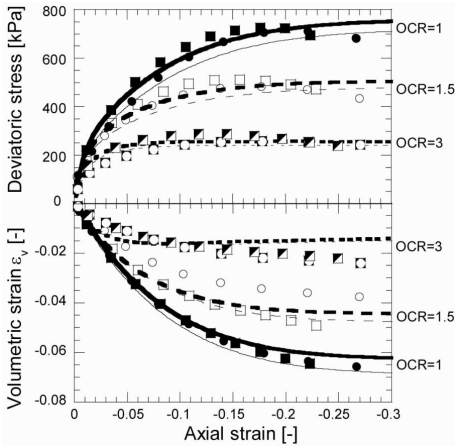


Fig. 5. Simulation of triaxial shear tests under different confining pressures ($p'_c = -600$ kPa). Circle (square) points: Experimental results at T = 22 °C (T = 90 °C) [18]. Thin (thick) lines: numerical simulations at T = 22 °C (T = 90 °C)

The second set of experiments consists of triaxial tests on kaolin clay at two different temperatures (22 °C and 90 °C) and under different OCR [18]. The cases of OCR = 1, 1.5 and 3 have been simulated at both temperatures. The comparison between the experimental and finite element results are depicted in Fig. 5 and reveal a good capability of the ACMEG-T model implemented in the COMES-GEO code to describe the thermal effects on the deviatoric response of soil, as observed experimentally. In particular, equation (6) coupled with equations (7) and (10) clearly shows that temperature induces a change in the deviatoric yield limit, through the modification of preconsolidation pressure and friction angle, and so modifies the stress-strain response of soil when temperature changes.

### 6.2. Boundary value problem

The following example aims to validate the finite element formulation

solving an initial boundary value problem. It deals with the simulation of a non-isothermal fully saturated consolidation problem, for which the numerical solution of the linear thermo-mechanical problem is known [15].

A column of 7 m height and 2 m width is subjected to an external surface compressive load of 1.0 kPa and to a surface temperature jump of 50 K above the initial ambient temperature of 293.15 K. The material is initially water saturated. The upper surface is drained ($p^w = 0$ Pa); the lateral and the bottom surfaces are insulated. Horizontal displacements are constrained along the vertical boundaries and vertical displacements are constrained at the bottom surface. The column is discretized by nine eight-node isoparametric elements (Fig. 6). Furthermore, $3 \times 3$ Gauss integration points are used. The material parameters used in the computation are listed in Table 2. Gravity forces are taken into account. Plane strain conditions are assumed.

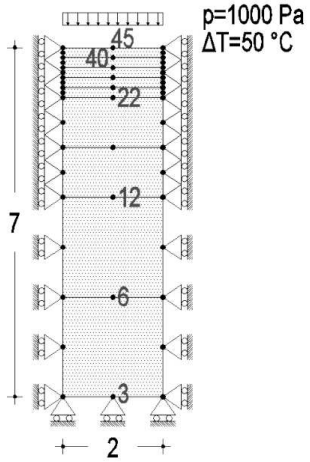


Fig. 6. Spatial discretisation and boundary conditions for the non-isothermal consolidation example

The case studied in [15], which assumed constant Young modulus ($E = 6.0$ MPa) and Poisson ratio ($\nu = 0.4$) and constant cubic thermal expansion coefficient, is used as validation example. To this aim, the results of [15] as published in [4] and labelled "Aboustit *et al.*" in the Figs 7 and 8, are used to compare the solution obtained with the finite element formulation proposed in this paper and labelled "ACMEG-T". The time histories for the water pressure (Fig. 7(a)), the temperature (Fig. 7(b)) and the vertical displacement (Fig. 7(c)) of several nodes of the mesh show the coincidence of the two solutions. The linear behaviour of the thermo-mechanical problem adopting the

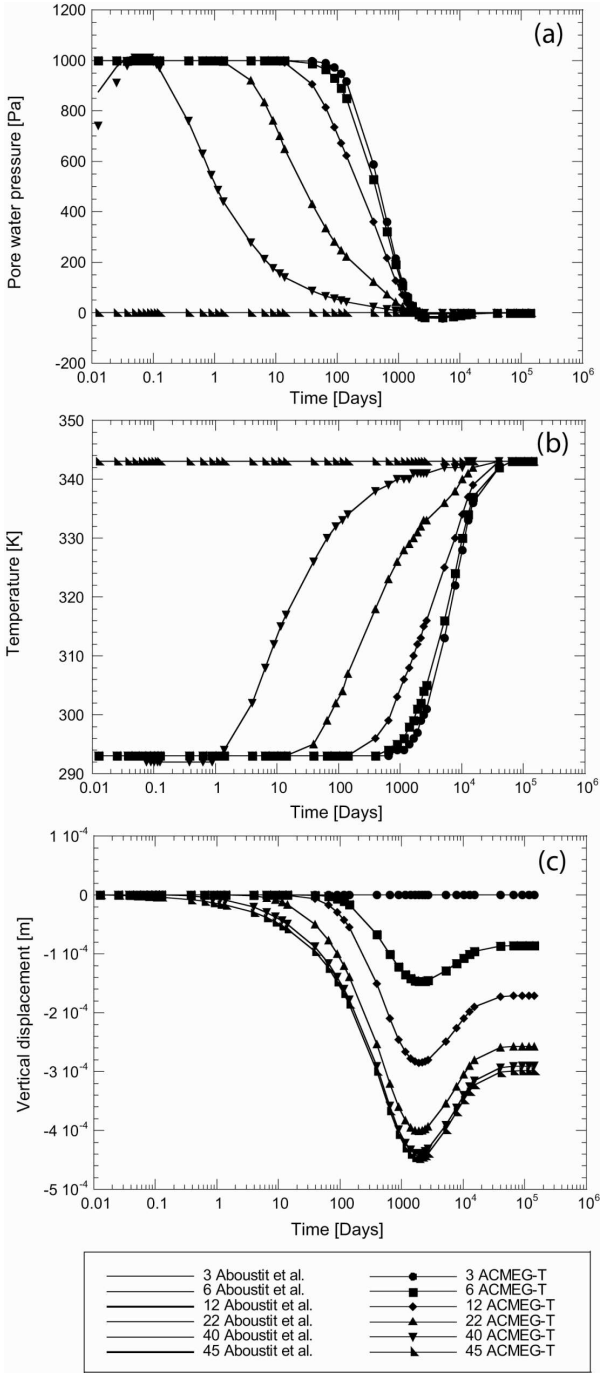


Fig. 7. Simulation of non-isothermal fully saturated consolidation problem using linear thermo-elasticity and comparison with results of [4]. Evolution of pore water pressure (a), temperature (b) and vertical displacement (c)

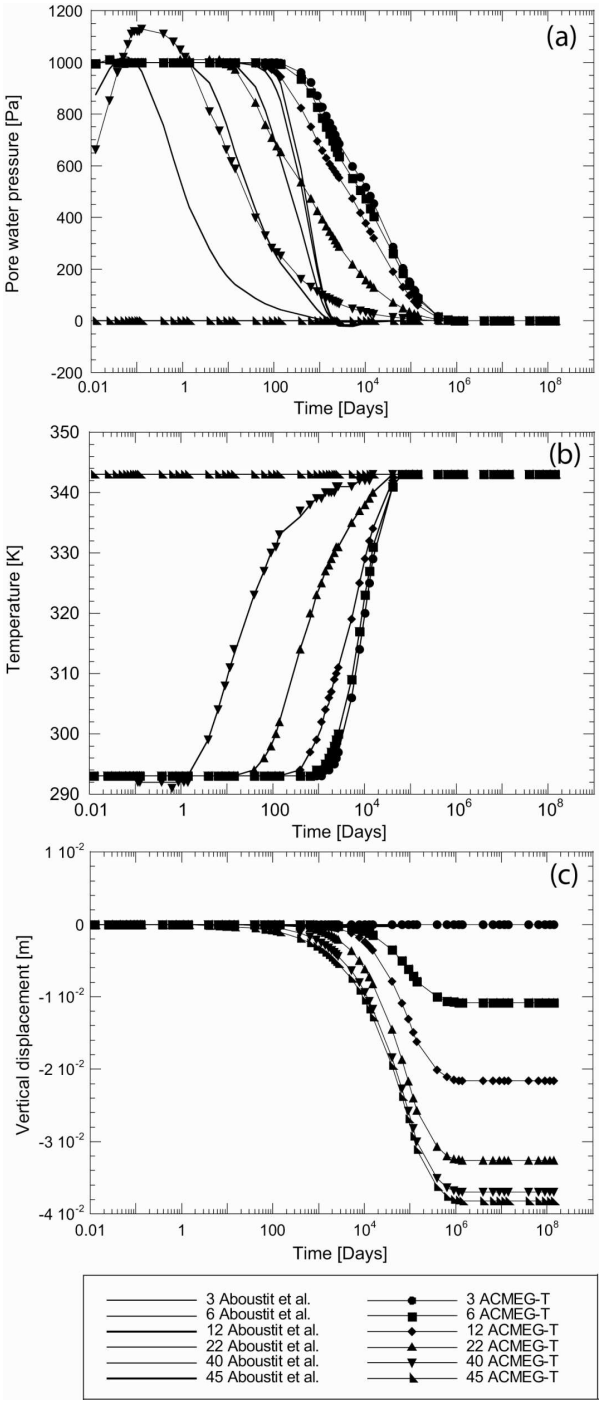


Fig. 8. Simulation of non-isothermal fully saturated consolidation problem using thermo-elastoplasticity and comparison with results of [4]. Evolution of pore water pressure (a), temperature (b) and vertical displacement (c)

ACMEG-T model is obtained by using the mechanical moduli independent of the stress state ($n^e = 0$).

As shown all along the present paper, soils are often subject to irreversible processes induced by thermal effect. In this context, the last simulation extends the problem of Fig. 6 towards thermo-elastoplastic analysis. The material parameters are listed in Table 2, where it can be observed that the linear elasticity is kept for comparison with the previous simulation; thermo-plasticity is introduced by reducing the preconsolidation pressure to get a mechanical and thermal hardening when loaded to 1 kPa and introducing the decrease of the isotropic yield surface with temperature.

The comparison between the elastic and the elasto-plastic solution shows that the inclusion of the plasticity effects delays the dissipation of pore water pressure in time (Fig. 8(a)), because of the reduced thermo-plastic stiffness of the solid skeleton with respect to the elastic one. Moreover, the predicted water pressures at the same time station are therefore higher than those from the elastic analysis.

Temperature evolution is almost not modified with respect to the previous simulation, as it can be observed in Fig. 8(b). Indeed, because parameters of thermal conduction and convection are almost independent of porosity changes, at least for this range of volumetric strain, equation (3) remains almost unaffected by mechanical change. On the contrary, the time history for the vertical displacements appears to be strongly affected by thermo-plastic behaviour of the solid skeleton. In particular, an increase of two order of magnitude for the vertical displacements is observed (Fig. 8(c)), that makes negligible the thermal component that can be observed in Fig. 7(c).

## 7. Conclusions

A coupled finite element formulation for thermo-elastoplastic water saturated geomaterials based on Porous Media Mechanics was presented. To this end, the ACMEG-T thermo-plastic constitutive model for saturated soils has been implemented in the finite element code COMES-GEO for the analysis of non-isothermal elastoplastic multiphase solid porous materials.

Validation of the implemented model was made by selected comparison between model simulation and experimental results for different combinations of thermo-hydro-mechanical loading paths. A case of non-isothermal elastic or elasto-plastic consolidation was solved.

The model has been obtained as a result of a research in progress on the thermo-hydro-mechanical modelling of multiphase geomaterials undergoing

inelastic strains. The validation case addressed in this paper remains very simple but clearly points out that with a sufficiently general thermo-hydro-mechanical model, the main THM couplings occurring in fine soils may be reproduced in a relevant manner. In particular, thermo-elastoplastic effects coupled with transient water and heat flow can be numerically analysed. That constitutes a powerful tool to address many geoenvironmental problems.

## REFERENCES


[1] Laloui, L., C. Cekerevac. Thermo-Plasticity of Clays: An Isotropic Yield Mechanism. *Computers and Geotechnics,* **30** (2003), 649–660.

[2] Laloui, L., C. Cekerevac, B. François. Constitutive Modelling of the Thermo-Plastic Behaviour of Soils. *Revue Européenne de Génie Civil*, **9** (2005), No. 5–6, 635–650.

[3] Sanavia, L., F. Pesavento, B. A. Schrefler. Finite Element Analysis of Non-isothermal Multiphase Geomaterials with Application to Strain Localization Simulation. *Computational Mechanics,* **37** (2006), No. 4, 331–348.

[4] Lewis, R. W., B. A. Schrefler. The Finite Element Method in the Static and Dynamic Deformation and Consolidation of Porous Media, J. Wiley, Chichester, 1998.

[5] Gawin, D., B. A. Schrefler. Thermo-Hydro-Mechanical Analysis of Partially Saturated Porous Materials. *Engineering Computations*, **13** (1996), No. 7, 113–143.

[6] Schrefler, B. A. Mechanics and Thermodynamics of Saturated-Unsaturated Porous Materials and Quantitative Solutions. *Applied Mechanics Review*, **55** (2002), No. 4, 351–388.

[7] Hassanizadeh, M., W. G. Gray. General Conservation Equations for Multi-Phase System: 1. Averaging Technique. *Adv. Water Res.*, **2** (1979), 131–144.

[8] Schrefler, B. A., L. Sanavia. Coupling Equations for Water Saturated and Partially Saturated Geomaterials. *Revue Française de Génie Civil*, **6** (2002), 975–990.

[9] Gawin, D., L. Sanavia. Modelling of Cavitation and Rapid Water Desaturation of Porous Media Considering Effects of Dissolved Air. *Transport in Porous Media* (Accepted).

[10] Laloui, L., B. François. ACMEG-T: A Comprehensive Soil Thermo-Plasticity Model. (Submitted).

[11] Hujeux, J. C. Une loi de comportement pour le chargement cyclique des sols, In: Génie Parasismique. Les éditions de l'E.N.P.C, Paris, 1985, 287–302.

[12] Prager, W. Non-Isothermal Plastic Deformation. *Koninkklijk-Nederland Akademie Van Wetenschappen Te Amsterdam – Proceedings of the Section of Sciences – B*, **61** (1958), 176–182.

[13] Rizzi, E., G. Maier, K. Willam. On Failure Indicators in Multi-Dissipative Materials. *International Journal of Solids and Structures*, **33** (1996), No. 20–22, 3187–3214.

[14] Simo, J. C., T. J. R. Hughes. Computational Inelasticity, Springer, New York, 1998.

[15] Aboustit, B. L., S. H. Advani, J. K Lee. Variational Principles and Finite Element Simulations for Thermo-Elastic Consolidation. *Int. J. Num. Anal. Meth. Geomech.*, **9** (1985), 49–69.

[16] Jamin, F. Contribution à l'étude du transport de matière et de la rhéologie dans les sols non saturés à différentes temperatures, PhD Thesis, Université Montpellier 2, 2003.

[17] Baldi, G., T. Hueckel, A. Peano, R. Pellegrini. Developments in Modelling of Thermo-Hydro-Geomechanical Behaviour of Boom Clay and Clay-Based Buffer Materials, Report: 13365/2 EN, Commission of the European Communities, 1991.

[18] Cekerevac,C., L. Laloui. Experimental Study of the Thermal Effects on the Mechanical Behaviour of a Clay. *International Journal of Numerical and Analytical Methods in Geomechanics*, **28** (2004), 209–228.